Article

Diamagnetic imaging agents with a modular chemical design for quantitative detection of #-galactosidase and #-glucuronidase activities with catalyCEST MRI

Gabriela Fernandez-Cuervo, Kirsten A Tucker, Scott W Malm, Kyle Mitchell Jones, and Mark D Pagel

Bioconjugate Chem., **Just Accepted Manuscript** • DOI: 10.1021/acs.bioconjchem.6b00482 • Publication Date (Web): 22 Sep 2016

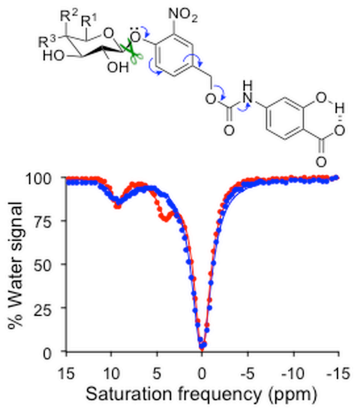
R2
R1
R3
HO
O
OH
NO2
O
O
H
N
O
O
O
H
O
O
100
75
50
25
0
% Water signal
15
10
5
0
-5
-10
-15
Saturation frequency (ppm)

Diamagnetic imaging agents with a modular chemical design for quantitative detection of β-galactosidase and β-glucuronidase activities with catalyCEST MRI

Gabriela Fernández-Cuervo,[†] Kirsten A. Tucker,[‡] Scott W. Malm,[§] Kyle M. Jones[‖] and Mark D. Pagel[*, ‡, ‖, □]

†*Department of Pharmaceutical Sciences, The University of Arizona, 1295 N Martin, P.O. Box 210202, Tucson AZ, 85721*
‡*Department of Chemistry and Biochemistry, The University of Arizona, 1306 E University Blvd, Tucson, AZ 85719*
§*Department of Pharmacology and Toxicology, The University of Arizona, 1295 N Martin, P.O. Box 210202, Tucson AZ, 85721*
‖ *Department of Biomedical Engineering, The University of Arizona, 1127 E James E. Rogers Way, P.O. Box 210020, Tucson, AZ 85721*
□*Department of Medical Imaging, The University of Arizona, 1515 N Campbell Avenue, Tucson AZ, 85724-5024*
** E-mail: mpagel@u.arizona.edu*

ABSTRACT: Imaging agents for the non-invasive *in vivo* detection of enzyme activity in preclinical and clinical settings could have fundamental implications in the field of drug discovery. Furthermore, a new class of targeted prodrug treatments takes advantage of high enzyme activity to tailor therapy and improve treatment outcomes. Herein we report the design and synthesis of new magnetic resonance imaging (MRI) agents that quantitatively detect β-galactosidase and β-glucuronidase activities by measuring changes in chemical exchange saturation transfer (CEST). Based on a modular approach, we incorporated the enzymes' respective substrates to a salicylate moiety with a chromogenic spacer *via* a carbamate linkage. This furnished highly selective diamagnetic CEST agents that detected and quantified enzyme activities of glycoside hydrolase enzymes. Michaelis-Menten enzyme kinetics studies were performed by monitoring catalyCEST MRI signals, which were validated with UV-vis assays.

Introduction

Understanding the functions of proteins in their innate *in vivo* tissue environment can provide useful biomarker information enabling appropriate and timely decisions with respect to drug development and the use of personalized therapy in routine clinical care.[1] For example, the detection of enzyme activity relative to detecting enzyme expression when evaluating preclinical assessments of new treatment strategies has proven to be crucial.[2] β-galactosidase (β-gal) and β-glucuronidase (β-gus) are glycoside hydrolase enzymes that have been employed in prodrug monotherapy (PMT),[3-11] antibody directed enzyme prodrug therapy (ADEPT)[12-17] and gene directed enzyme prodrug therapy (GDEPT).[18-21] Despite the appealing concept of targeted prodrug therapies, these treatment strategies have yielded inconsistent results throughout the past decade, potentially due to variable levels of β-gal and β-gus activities in tissues. The evaluation of β-gal and β-gus activities within *in vivo* tissues would improve our understanding of these treatment strategies and improve the paradigm of personalized medicine by identifying patients who could benefit from prodrugs that employ these enzymes.

Significant chemical efforts have been invested to develop new and improved biomedical imaging agents that detect enzyme activity within *in vivo* tissues.[22] In particular, chemical agents have been developed that detect the activities of β-gal and β-gus with fluorescence,[23-24] luminescence,[25] chemiluminiscence[26] and optoacoustic[27] imaging. However, these techniques suffer from poor spatial resolution and/or depth of view *in vivo*. PET and SPECT agents have been designed that are retained in tissues after cleavage by β-gal or β-gus.[28-32] These radionuclide agents depend on the relative pharmacokinetics of the agent before and after cleavage, which may be influenced by many other physiological conditions, compromising the detection of enzyme activity. ^{19}F NMR spectroscopy can show a change in chemical shift after enzyme cleavage, however ^{19}F-NMR is insensitive and equipment is lacking in the clinic.[33] MRI contrast agents have been developed that non-invasively detect β-gal and β-gus by changing their T_1 relaxation time constant of the agent when cleaved by these enzymes.[34-35] Unfortunately, the concentration of the agent and other experimental conditions affect the T_1 time measured by MRI, which compromises the specificity for detecting these enzymes. Moreover, even though some agents rely on a shift in signal, most of these agents only count with one on/off signal, making it challenging to conduct controlled measurements. Therefore, a new imaging method and improved contrast agents are needed to detect β-gal and β-gus activities.

A new type of MRI contrast generated by Chemical Exchange Saturation Transfer (CEST) can be exploited for molecular imaging.[36] CEST MRI requires a labile proton on an agent with a relatively slow chemical exchange rate that can be selectively saturated while avoiding direct saturation of the MR frequency of water. This selective saturation greatly reduces the net magnetization of the agent's proton pool, thus eliminating the detectable MR signal from these protons. These saturated protons exchange with bulk water and in turn decrease the water signal amplitude (Figure 1). Continuous selective saturation at the MR frequency of the agent's labile proton can build a large population of saturated water protons which greatly improves detection sensitivity.

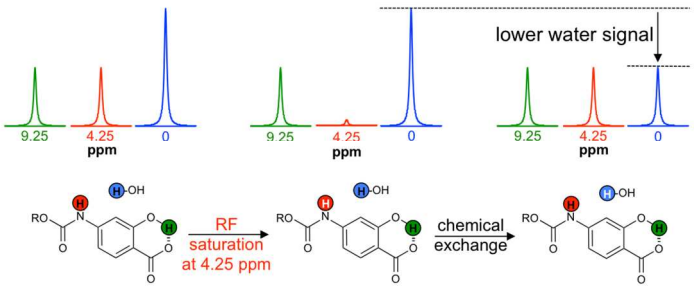

Figure 1. CEST MRI Mechanism. Radio frequency saturation of the carbamide hydrogen atom (green) results in the loss of the MRI signal (a saturated proton is shown in white). After exchanging this saturated hydrogen atom with a hydrogen atom on water (blue), some of the MRI signal of water is lost, which can be measured with MRI. The MRI signal of the proton of the salicylic acid moiety (green) is unchanged because chemical exchange with saturated carbamide or saturated water protons is negligible. However, radio frequency saturation of the salicylic acid proton would cause a similar decrease in the water signal based the same mechanism.

We have developed an imaging protocol, termed catalyCEST MRI, that can detect enzyme activity *in vitro*[37-43] and *in vivo*.[44-45] CatalyCEST MRI simultaneously detects enzyme-responsive and unresponsive "control" CEST signals, and uses the ratio of the signals to detect enzyme activity with outstanding specificity relative to other conditions that affect CEST MRI. Dual-signal CEST MRI contrast agents have been developed that are substrates for esterase,[39] cathepsin B,[42] sulfatase,[43] urokinase Plasminogen Activator,[44] and γ-glutamyl transferase[45] enzymes. Some of these agents are based on the chemical structure of salicylic acid, which provides an exchangeable proton source with an excellent chemical shift for selective saturation. Moreover, branching from the amino group of the amino salicylic acid analogue provides a second CEST proton source for the agent, which would furnish a single agent that simultaneously detects two CEST signals. Overall, these properties in addition to good biocompatibility make this scaffold an excellent potential candidate for clinical translation.[46] Derivatives of salicylic acid are relatively accessible and enzyme responsive contrast agents can be easily synthesized by conjugating an enzyme's substrate directly to the salicylate moiety.

Unfortunately, many enzymes may be inactive or have sluggish activity when catalyzing the cleavage to a substrate that is directly linked to an imaging agent. Both β-gal and β-gus suffer from this pitfall, as evidenced by the poor catalytic cleavage of a glycoside substrates resulting in limited prodrug activation.[47] In particular, the pKa of the alkyl alcohol leaving group of the substrate can influence the activity of these enzymes.[48-50] Therefore, we sought to expand this platform technology by incorporating a spacer between the salicylate and glycoside moieties *via* a carbamate linkage, creating a "tri-modular" scaffold that would extend salicylic acid from the enzyme substrate and avoid steric hindrance (Scheme 1a). Additionally, having an electron withdrawing substituent at the alkoxy leaving group provides further stabilization of the galactosyl-enzyme intermediate thus improving cleavage. A similar approach has been used to develop other prodrugs[51] suggesting that this approach is feasible for developing diamagnetic CEST agents.

Our selection of a nitrobenzyloxy-carbamate moiety was inspired by the use of a similar spacer that was incorporated into a paramagnetic CEST agent that detected β-gal activity.[52-53] This type of spacer can spontaneously disassemble upon enzyme cleavage of the pyranose from the agent. This disassembly converted the carbamate to an amine on the paramagnetic agent, which caused the appearance of two CEST signals at -16.7 and -20.5 ppm that were used to detect enzyme activity. In our approach, the disassembly of the carbamate spacer is designed to cause a disappearance of the CEST signal from the carbamate, while the CEST signal from the salicylate moiety remains as an enzyme-unresponsive control signal (Scheme 1b). The comparison of enzyme-responsive and unresponsive CEST signals is an improvement in the design of agents for catalyCEST MRI. Furthermore, we used a carbamate spacer bearing a nitro group that more rapidly disassembles than the spacer used in the paramagnetic agent, which can improve the temporal response to enzyme activity. Finally, our diamagnetic agent is designed to retain large chemical shifts without requiring a paramagnetic ion that is potentially toxic at high concentrations, which provides yet another advantage.

As an additional advantage, the selected spacer generates an optically active product after the spontaneous disassembly. Validation of molecular imaging probes is a major requirement for developing biochemical imaging agents, and the generation of an optical signal after β-gal or β-gus activity can provide this essential validation. Optical imaging is more rapid and economical relative to MRI, which facilitates straightforward validation studies in solution.

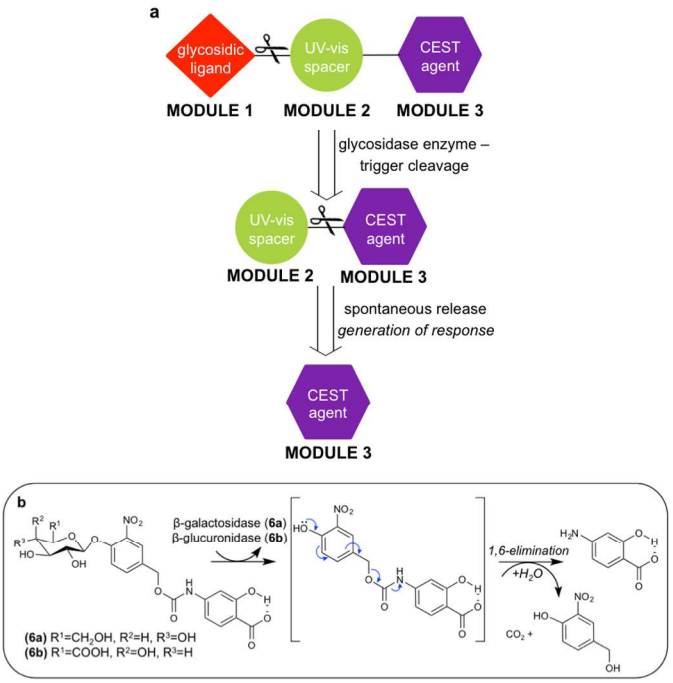

Scheme 1. (a) Modular design of the CEST MRI agent. (b) The proposed release mechanism of the enzyme responsive contrast agent.

Results and discussion

Design of enzyme-responsive CEST MRI agents for detecting β-gal or β-gus activity

To synthesize our agent, the spacer **1** was conjugated to the corresponding activated bromo-glycosides **2a** and **2b**, through a Koenigs-Knorr glycosylation reaction to furnish **3a** and **3b** (Scheme 2). Compounds **3a** and **3b** were then conjugated to **4** through a carbamate linkage between these moieties. In a two-step one-pot reaction, the amino group was converted into an isocyanate group in the presence of triphosgene, and subsequently reacted with the hydroxyl group of compounds **3**. (Triphosgene is toxic and corrosive; MSDS must be consulted prior to use). The final step followed a suitable Zemplén deacetylation reaction to provide imaging agents **6a** and **6b** in good yields. More details about the synthesis and the studies described below can be found in the Supporting Information.

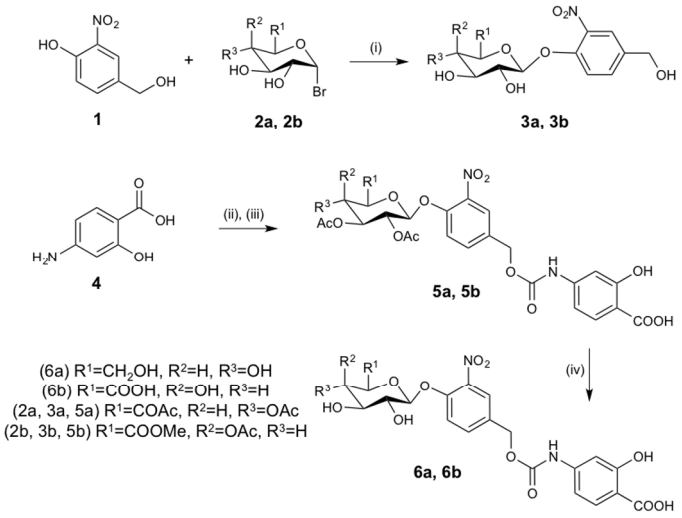

Scheme 2. (i) Silver oxide, ACN, room temperature, 2 h, 86% (**3a**), 88% (**3b**). (ii) Triphosgene, 1:1 ACN/toluene, 60 °C to 80 °C, 2h. (iii) 3, 80 °C, 1 h, 13% (**5a**), 34% (**5b**). (iv) MeOH, NaOMe, room temperature, 30 min, 47% (**6a**), 83% (**6b**).

Detection of enzyme catalysis

We detected the activity of β-gal or β-gus by acquiring CEST spectra from each agent before and after adding enzyme (Figure 2a,c). Before enzyme hydrolysis, we observed two CEST signals from each agent at 9.25 ppm and 4.25 ppm, corresponding to the selective saturation of the exchangeable proton from the salicylate and the carbamate moieties, respectively. In the presence of enzyme, the signal at 4.25 ppm disappeared, corresponding to the conversion of the agent into 4-amino salicylic acid as a consequence of catalytic hydrolysis of the glycosidic ligand. The signal of the agent at 9.25 ppm did not change in amplitude. However, this signal showed a slight decrease in saturation frequency after enzyme cleavage due to the decoupling of the electron withdrawing carbamate from the salicylic acid moiety. Importantly, the ratio of the CEST peaks effectively detected enzyme activity in a concentration–independent manner. This result demonstrated the responsiveness of this agent for each enzyme.

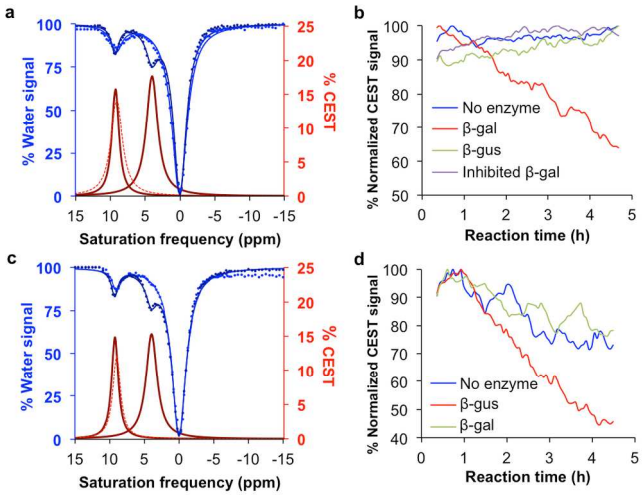

Figure 2. catalyCEST MRI. (a) The experimental CEST spectra (blue circles), the Lorentzian line fitting of the experimental CEST spectra (blue lines), and the Lorentzian line shapes showed two CEST signals from the substrate **6a** (solid red lines) and only one CEST signal for the product after β-gal catalysis (dashed red line). (b) The normalized CEST signal at 4.25 ppm decreased after treatment of **6a** with β-gal (red). No change in CEST signal was observed after treatment with β-gus (green), with β-gal inhibited by PETG (purple), or in the absence of enzyme (blue). (c) and (d) Similar results were obtained before and after enzyme catalysis of **6b** with β-gus.

We performed additional studies for both enzymes to further validate that the change in CEST signal was due to enzyme activation. Because the CEST effect at 4.25 ppm represents substrate before cleavage, we monitored this CEST signal over 4.5 hours (Figure 2b,d). The CEST signal decreased in the presence of the corresponding enzyme for each agent. This CEST signal of agent **6a** remained

consistently high in the presence of inhibited β-gal, implying that this agent truly detects β-gal activity. The CEST signal of **6a** also remained high in the absence of β-gal, demonstrating that this agent is stable in solution. The CEST signal was also consistently high for **6a** treated with β-gus, indicating excellent specificity for detecting β-gal versus β-gus. The CEST signal for agent **6b**, with no enzyme, showed a slow decrease suggesting that the agent was slightly unstable in the buffer conditions that were tested. The addition of β-gal to the agent in these buffer conditions did not accelerate the rate signal decrease compared to the control, suggesting β-gal did not cleave the agent, thus indicating good specificity for **6b** to detect β-gus against β-gal.

To further verify these results, LC-MS analysis revealed that the glycosidic cleavage led to the anticipated 1,6-elimination and the release of both reporters, 4-hydroxy-3-nitrobenzyl alcohol spacer, and 4-amino salicylic acid (Figure S1, S2). Qualitative confirmation of enzyme activity was noted as the solution became yellow after enzyme cleavage. As additional validation the liberation of 4-hydroxy-3-nitrobenzyl alcohol (**1**) was detected by UV-vis absorbance at 425 nm (Figure S3). The 3.8- and 10.9-fold increase in optical absorbance after treatment with β-gal or β-gus, respectively, demonstrated that the agent had excellent detection sensitivity for confirming the activity of these two enzymes in solution.

Optimization of catalyCEST MRI parameters

We used the HW-QUESP method to evaluate the dependence of CEST signal amplitude on saturation power.[54] A saturation power of 4 μT was shown to generate relatively strong CEST signals from the agent while still maintaining an acceptably low power below the SAR limit for *in vivo* studies (Figure S4, S5). We used the RL-QUEST method to assess the effect of the saturation time on CEST signals.[55] A saturation time of 3 seconds was adequate for generating strong CEST signal amplitude from each agent while maintaining a relatively short acquisition time for eventual *in vivo* studies (Figure S6, S7).

We evaluated the chemical exchange rates (k_{ex}) of **6a** and **6b**, using a HW-QUESP CEST MRI analysis method (Figure S4, S5). The carbamide proton had a k_{ex} of 701 Hz and 693 Hz for **6a** and **6b**, respectively, and the salicylate proton's k_{ex} was 972 Hz and 1007 Hz for **6a** and **6b**. These k_{ex} values for the salicylate proton of the substrate agents were similar to the k_{ex} of the product, which was determined to be 934 Hz in a previous study.[45] These similar k_{ex} values of the substrates and product showed that the salicylate generated an enzyme-unresponsive "control" signal to improve the evaluation of enzyme activity. As expected, the k_{ex} of the salicylic acid proton and the carbamide proton were slower than the saturation frequency of each proton (2,775 Hz at 9.25 ppm, and 1,275 at 4.25 ppm, at 300 MHz magnetic field strength), which is a requirement for good CEST detection.

Michaelis-Menten kinetics analysis

We performed Michaelis-Menten enzyme kinetics studies to quantitatively demonstrate that our agents detect enzyme activity.[38] Samples of the agents ranging from 4 mM to 50 mM were treated with each enzyme and 75 CEST spectra were acquired for 4.5 hours (Figure 3a,d). The temporal disappearance of the CEST signal at 4.25 ppm was converted to concentration of the uncleaved agent at each time point of the reaction, using our previously determined HW-Conc CEST calibration method with an identical CEST MRI protocol (Figure 3b,e).[56] The initial velocity of each reaction, v_i, was determined from the rate of decrease of the uncleaved agent's concentration during the first 2 hours of the reaction. The good fitting of the Hanes- Woolf plot to the experimental results ($R^2 = 0.80$ for β-gal and 0.76 for β-gus) demonstrated that the CEST agent followed Michaelis-Menten kinetics and therefore was responsive to enzyme activity (Figure 3c,f). These plots were used to determine the reaction velocity, V_{max}, Michaelis constant, K_M, catalysis rate, k_{cat}, and the catalytic efficiency, k_{cat}/K_M for each enzyme (Table 1).

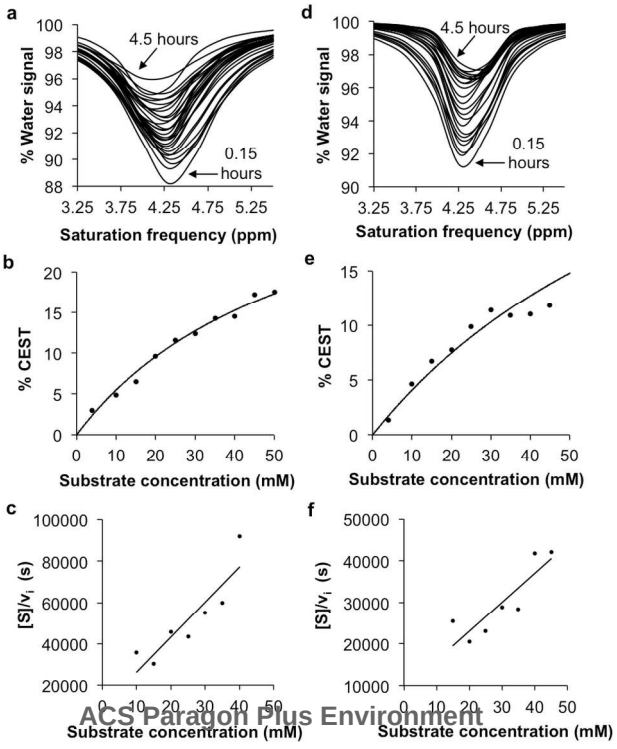

Figure. 3 Michaelis-Menten kinetics studies with catalyCEST MRI. (a) The decrease of the CEST signal at 4.25 ppm was monitored for 4.5 hours with catalyCEST MRI after adding 0.25 units of β-gal to 25 mM of **6a**. (b) The CEST signal amplitude was correlated with the concentration of **6a** using the HW-Conc analysis method. The initial velocity, v_i, was determined by converting the CEST signal in panel a to concentration, using the calibration curve in panel b. (c) A Hanes-Woolf plot was used to determine Michaelis-Menten kinetics parameters. (d-f) This analysis was repeated for evaluating the kinetics of β-gus with its substrate **6b**.

We repeated Michaelis-Menten kinetics studies of the agents **6a** and **6b** by monitoring the optical density of the spontaneously disassembling spacer (Figure 4, Table 1). We converted the optical density to concentration using a Beer-Lambert correlation with 4-hydroxy-3-nitrobenzyl alcohol (**1**) as the standard for both agents. The initial velocity, v_i, was determined from the increasing rate of 4-hydroxy-3-nitrobenzyl alcohol concentration produced from the liberation of free spacer during the first 2 and 1 hours of the cleavage of **6a** and **6b** by their respective enzymes. We used the Hanes-Woolf plot to determine Michaelis-Menten kinetics constants to directly compare results from the catalyCEST MRI experiment. The minor curvature in the Hanes-Woolf plot for β-gus suggested a systematic error in the kinetics analysis. This error was attributed to the competitive inhibition of the β-gus enzyme by glucuronic acid, which is a product of the reaction.[57]

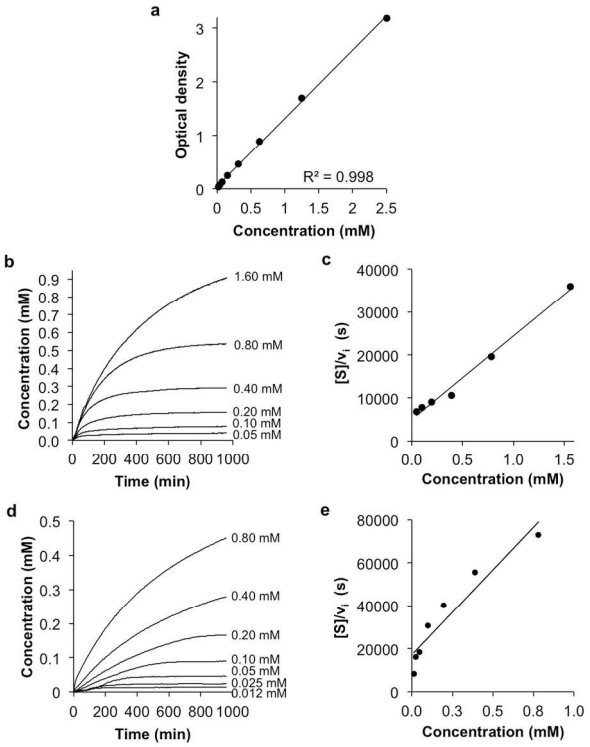

Figure. 4 Michaelis-Menten kinetics studies with absorbance at 425 nm. (a) The absorbance at 425 nm was correlated with the concentration of 4-hydroxy-3-nitrobenzyl alcohol (**1**) using the Beer-Lambert law. (b) The initial velocity, v_i, was determined by monitoring the change in UV absorbance of **6a** after adding β-gal enzyme, and converting the absorbance at 425 nm to concentration using the calibration in panel a. (c) A Hanes-Woolf plot with initial velocities and substrate concentrations was used to determine Michaelis-Menten kinetics parameters. (d) and (e) This analysis was repeated for evaluating the kinetics of β-gus with its substrate **6b**.

For agent **6a** responsive to β-gal, the K_M, k_{cat} and catalytic efficiency constants were comparable within an order of magnitude between the analyses performed with catalyCEST MRI and UV-vis studies. This order of magnitude comparison is reasonable considering that MRI techniques are less precise than optical techniques. This result provided confidence that catalyCEST MRI can quantitatively evaluate enzyme activity. For agent **6b** responsive to β-gus, the K_M and k_{cat} values differed by about two orders of magnitude between each analysis method. This difference was attributed to the minor systematic error caused by the competitive inhibition of β-gus by free glucuronic acid. This competitive inhibition has a stronger influence on the UV-vis analysis than catalyCEST MRI that sustains saturation of the enzyme with a substrate for a longer time. Furthermore, the systematic error was cancelled by the Hanes-Woolf analysis method when determining the catalytic efficiency, which explains why the catalytic efficiencies, k_{cat}/K_M, determined by the catalyCEST MRI and UV-vis analyses are similar, despite differences in K_M and k_{cat} values.

Table 1. Michaelis-Menten kinetics constants.

Michaelis-Menten	β-galactosidase-responsive agent (**6a**)			β-glucuronidase-responsive agent (**6b**)		
Enzyme Kinetics	catalyCEST MRI	UV-vis	MRI/UV-vis	catalyCEST MRI	UV-vis	MRI/UV-vis
V_{max}	58.9×10^{-8} M s^{-1}	5.16×10^{-8} M s^{-1}	11.4	143×10^{-8} M s^{-1}	1.26×10^{-8} M s^{-1}	113
k_{cat}	12.3×10^{1} s^{-1}	2.16×10^{1} s^{-1}	5.7	128×10^{-1} s^{-1}	1.13×10^{-1} s^{-1}	113
K_M	54.9×10^{-4} M	2.60×10^{-4} M	21.1	131×10^{-4} M	2.16×10^{-4} M	60.6
k_{cat}/K_M	2.24×10^{4} M^{-1} s^{-1}	8.32×10^{4} M^{-1} s^{-1}	0.27	9.80×10^{2} M^{-1} s^{-1}	5.21×10^{2} M^{-1} s^{-1}	1.88

Based on the Michaelis-Menten kinetics analysis, β-gal and β-gus had similar K_M constants for the respective contrast agent, demonstrating similar binding affinities for their ligands. β-gal has a faster k_{cat} value than β-gus. The rate of the spontaneous disassembly of the spacer should be identical for **6a** and **6b** after cleavage of the glycosidic ligand, so the faster k_{cat} of β-gal indicates faster glycosidic

cleavage of **6a**. Coupled with the evidence that glucuronic acid can be a competitive inhibitor for the β-gus enzyme, agent **6a** and β-gal appear to be the better choice for subsequent application of *in vitro* and *in vivo* imaging with catalyCEST MRI.

In conclusion, we have shown that diamagnetic CEST agents can detect and quantify the enzyme activities of glycoside hydrolase enzymes. The implementation of a modular design facilitated agent activation and thus detection of both enzymes. Incorporating the spontaneously disassembling spacer provided a tri-modular design for detecting enzyme catalysis. Additionally, we took advantage of this spacer to incorporate a chromophore moiety that validated our MRI studies with UV-vis studies. These CEST MRI agents were also used to test substrate specificity and assess enzyme inhibition, which expands the utility of catalyCEST MRI as a platform technology for enzyme studies. Based on our kinetics results, β-gal has superior catalysis properties relative to β-gus for this class of modular catalyCEST MRI contrast agents.

These findings demonstrate that the newly synthesized modular agents **6a** and **6b** have the potential to become a reliable catalyCEST MRI imaging probe for the non-invasive quantitative detection of enzyme activities. In addition, our results suggest that studies involving *in vitro* validation and *in vivo* translation are warranted. Such techniques may facilitate the identification and validation of new prodrugs that are activated by β-gal or β-gus. Moreover, the modular design of these agents facilitates the conjugation of other enzyme substrates to the carbamate spacer, so that this approach constitutes a platform technology for the detection of enzyme activity.

Experimental Procedures

Synthesis of enzyme-responsive CEST agents. The CEST agents were synthesized as described in the Supporting Information. Compounds were analyzed with ^{1}H and ^{13}C NMR spectroscopic methods using a Bruker Avance-III 400 MHz NMR spectrometer. Final products were confirmed with high-resolution electrospray ionization (HRMS (ESI negative mode)) mass spectroscopy analysis recorded with a Bruker 9.4 T Apex-Qh hybrid Fourier transfer ion-cyclotron resonance (FT-ICR) instrument. All compounds where purified by flash column chromatography when needed. Full characterization is provided in the Supporting Information.

Enzyme reactions. β-gal and β-gus from *E. coli* were purchased from Sigma Aldrich as lyophilized. Samples of the agents were prepared as shown in Table S1 of the Supporting Information. The substrate concentrations were varied between 4 – 50 mM and 0.050 – 3.125 mM, depending on the experiment and detection method. The temperature was adjusted to 37.0 ± 0.2 ^{o}C for enzyme incubation and for image acquisition in MRI and UV-vis experiments. Samples were analyzed after enzyme reactions with reverse phase LC-MS (Shimadzu Corp.) to verify enzyme hydrolysis.

CEST MRI acquisition protocol for the detection of enzyme catalysis. MRI studies were performed with a preclinical Bruker Biospec MRI scanner operating at 7.05 T (300 MHz) magnetic field strength with a 72 mm quadrature transceiver coil. A CEST-FISP acquisition protocol was used for all CEST MRI studies.[41] We acquired a series of 107 images after selective saturation was applied using a continuous wave pulse at 3 μT power for 4 s with frequencies ranging from 15 to -15 ppm. FISP acquisition parameters included TR: 3.196 ms; TE: 1.598 ms; excitation flip angle: 30°; centric encoding; number of averages: 1; matrix: 128x128; field of view: 6.4x6.4 cm; in-plane spatial resolution: 500x500 mm; slice thickness: 1 mm. The temporal resolution of acquiring one image with one selective saturation frequency was 5.441 s. The total time to acquire 107 images for a full CEST spectrum was 9:42 min.

CEST MRI acquisition protocol for Michaelis-Menten Kinetics studies. 75 image sets to generate a 62-point CEST spectrum were collected after selective saturation was applied using a continuous wave pulse at 3 μT power for 4 s with frequencies ranging from 15 to -15 ppm. The same FISP parameters were used for consistency. The total acquisition time was 4.5 hours.

Analysis of CEST spectra. A region of interest in the image of each sample was selected from the acquired image to generate a CEST spectrum for the sample. To measure CEST signal amplitudes, the spectrum was analyzed by fitting three Lorentzian line shapes to account for the direct saturation of water and the CEST signals at 4.25 ppm and 9.25 ppm.[41] The center, width and amplitude of each Lorentzian line shape were allowed to change to optimize the fit. The Lorentzian line shape fitting automatically referenced the bulk water chemical shift at 0 ppm, negating the effect of B_0 inhomogeneities in the CEST MR images.

UV-vis enzymatic microplate assays. Serial dilutions of appropriate substrate were incubated with 0.125 U of β-gal or 250 U of β-gus enzyme at 37.0 °C for 16 hours. Formation of product was detected in a Synergy HTX multi-mode plate reader (BioTek, Winooski, VT) at 425 nm every 2 minutes.

Associated Content

Supporting Information

The Supporting Information is available free of charge on the ACS Publications website at DOI:

Author Information

Corresponding Author

** E-mail: mpagel@u.arizona.edu. Phone: +1 520-404-7049*

Acknowledgements

The authors thank Edward A. Randtke, John Jewett, Kristen Keck and Walter Klimecki for helpful interactions. Gabriela Fernández-Cuervo is a Howard Hughes Medical Institute Gilliam Fellow also supported by the Biological Chemistry Program Training Grant: T32 GM008804. This research study was also funded by the NIH through grant R01 CA169774 and P01 CA95060.

Abbreviations

β-gal, β-galactosidase; β-gus, β-glucoronidase; CEST, chemical exchange saturation transfer; FISP, fast imaging with steady-state precession; LC-MS, liquid chromatography-mass spectrometry; MeOH, methanol; MRI, magnetic resonance imaging; NaOMe, sodium methoxide; NMR, nuclear magnetic resonance; PET, positron emission tomography; PETG, phenylethyl β-d-thiogalactoside; SPECT, single photon emission computed tomography; UV, ultraviolet

References

(1) Baruch, A., Jeffery, D. A., and Bogyo, M. (2004) Enzyme activity – it's all about image. *Trends in Cell Biology 14*, 29-35.

(2) Glanemann, C., Loos, A., Gorret, N., Willis, L. B., O'Brien, X. M., Lessard, P. A., and Sineskey, A. J. (2003) Disparity between changes in mRNA abundance and enzyme activity in *Corynebacterium glutamicum:* implications for DNA microarray analysis. *Appl. Microbiol. Biotechnol. 61*, 61-68.

(3) de Graaf, M., Boven, E., Scheeren, H. W., Haisma, H. J., and Pinedo, H. M. (2002) Beta-glucuronidase mediated drug release. *Curr. Pharm. Des. 8*, 1391-1403.

(4) Chen, X., Wu, B., and Wang, P. G. (2003) Glucuronides in anti-cancer therapy. *Curr. Med. Chem. Anticancer Agents 3*, 139-150.

(5) Houba, P. H., Boven, E., van der Meulen-Muileman, I. H., Leenders, R. G., Scheeren, J. W., Pinedo, H. M., and Haisma, H. J. (2001) A novel doxorubicin-glucuronide prodrug DOX-GA3 for tumour-selective chemotherapy: distribution and efficacy in experimental human ovarian cancer. *Br. J. Cancer 84*, 550-557.

(6) Schmidt, F., and Monneret, C. (2003) Prodrug Mono Therapy: synthesis and biological evaluation of an etoposide glucuronide-prodrug. *Bioorg. Med. Chem. 11*, 2277-2283.

(7) Angenault, S., Thirot, S., Schmidt, F., Monneret, C., Pfeiffer, B., and Renard, P. (2003) Cancer chemotherapy: a SN-38 (7-ethyl-10-hydroxycamptothecin) glucuronide prodrug for treatment by a PMT (Prodrug MonoTherapy) strategy. *Bioorg. Med. Chem. Lett. 13*, 947-950.

(8) Prijovich, Z. M., Chen, B. M., Leu, Y. L., Chern, J. W., and Roffler, S. R. (2002) Anti-tumour activity and toxicity of the new prodrug 9-aminocamptothecin glucuronide (9ACG) in mice. *Br. J. Cancer 86*, 1634-1638.

(9) Tietze, L. F., Herzig, T., Fecher, A., Haunert, F., and Schuberth, I. (2001) Highly selective glycosylated prodrugs of cytostatic cc-1065 analogues for antibody-directed enzyme tumor therapy. *Chembiochem 2*, 758-765.

(10) Bouvier, E., Thirot, S., Schmidt, F., and Monneret, C. (2004) First enzymatically activated Taxotere prodrugs designed for ADEPT and PMT. *Bioorg. Med. Chem. 12*, 969-977.

(11) Alaoui, A. E., Saha, N., Schmidt, F., Monneret, C., and Florent, J. C. (2006) New Taxol (paclitaxel) prodrugs designed for ADEPT and PMT strategies in cancer chemotherapy**.** *Bioorg. Med. Chem. 14*, 5012-5019.

(12) Haisma, H. J., van Muijen, M., Pinedo, H. M., and Boven, E. (1994) Comparison of two anthracycline-based prodrugs for activation by a monoclonal antibody-beta-glucuronidase conjugate in the specific treatment of cancer. *Cell Biophys. 24*, 185-192.

(13) Leu, Y. L., Roffler, S. R., and Chern, J. W. (1999) Design and synthesis of water-soluble glucuronide derivatives of camptothecin for cancer prodrug monotherapy and antibody-directed enzyme prodrug therapy (ADEPT). *J. Med. Chem. 42*, 3623-3628.

(14) de Bont, D. B., Leenders, R. G., Haisma, H. J., van der Meulen-Muileman, I. H., and Scheeren, H. W. (1997) Synthesis and biological activity of beta-glucuronyl carbamate-based prodrugs of paclitaxel as potential candidates for ADEPT. *Bioorg. Med. Chem. 5*, 405-414.

(15) Wang, S. M., Chern, J. W., Yeh, M. Y., Ng, J. C., Tung, E., and Roffler, S. R. (1992) Specific activation of glucuronide prodrugs by antibody-targeted enzyme conjugates for cancer therapy. *Cancer Res. 52*, 4484-4491.

(16) Tietze, L. F., Schuster, H. J., Krewer, B., and Schuberth, I. (2009) Synthesis and biological studies of different duocarmycin based glycosidic prodrugs for their use in the antibody-directed enzyme prodrug therapy. *J. Med. Chem. 52*, 537-543.

(17) Devalapally, H., Navath, R. S., Yenamandra, V., Akkinepally, R. R., and Devarakonda, R. K. (2007) Beta-galactoside prodrugs of doxorubicin for application in antibody directed enzyme prodrug therapy/prodrug monotherapy. *Arch. Pharm. Res. 30*, 723-732.

(18) Weyel, D., Sedlacek, H. H., Muller, R., and Brusselbach, S. (2000) Secreted human beta glucuronidase: a novel tool for gene-directed enzyme prodrug therapy. *Gene Ther. 7*, 224-231.

(19) de Graaf, M., Pinedo, H. M., Oosterhoff, D., van der Meulen-Muileman, I. H., Gerritsen, W. R., and Haisma, H. J. (2004) Pronounced antitumor efficacy by extracellular activation of a doxorubicin-glucuronide prodrug after adenoviral vector-mediated expression of a human antibody-enzyme fusion protein. *Hum. Gene Ther. 15*, 229-238.

(20) Carruthers, K. H., Metzger, G., During, M. J., Muravlev, A., Wang, C., and Kocak, E. (2014) Gene-directed enzyme prodrug therapy for localized chemotherapeutics in allograft and xenograft tumor models. *Cancer Gene Ther. 21*, 434-440.

(21) Fang, L., Battisti, R. F., Cheng, H., Reigan, P., Xin, Y., and Shen, J. (2006) Enzyme specific activation of benzoquinone ansamycin prodrugs using antibody-β-galactosidase conjugates. *J. Med. Chem. 49*, 6290-6297.

(22) Elias, D. R., Thorek, D. L. J., Chen, A. K., Czupryna, J., and Tsourkas, A. (2008) *In vivo* imaging of cancer biomarkers using activatable molecular probes. *Cancer Biomark. 4*, 287-305.

(23) Kobayashi, H., and Choyke, P. L. (2011) Target-cancer-cell-specific activable fluorescence imaging probes: rational design and *in vivo* applications. *Acc. Chem. Res. 44*, 83-90.

(24) Tung, C. H., Zeng, Q., Shah, K., Kim, D. E., Schellingerhout, D., and Weissleder, R. (2004) *In vivo* imaging of beta-galactosidase activity using far red fluorescent switch. *Cancer Res. 64*, 1579-1583.

(25) Wehrman, T. S., von Degenfeld, G., Krutzik, P. O., Nolan, G. P., and Blau, H. M. (2006) Luminiscent imaging of β-galactosidase activity in living subjects using sequential reporter-enzyme luminescence. *Nature Methods 3,* 295-301.

(26) Liu, L., and Mason, R. P. (2010) Imaging β-galactosidase activity in human tumor xenografts and transgenic mice using chemiluniscent substrate. PLoS ONE 5(8): e12024.
(27) Li, L., Zhang, H. F., Zemp, R. J., Maslov, K., and Wang, L. (2008) Simultaneous imaging of a lacZ-marked tumor and microvasculature morphology *in vivo* by dual-wavelength photoacoustic microscopy. *J. Innov. Opt. Health Sci. 1,* 207-215.
(28) Celen, S., Deroose, C., de Groot, T., Chitneni, S. K., Gijsbers, R., Debyser, Z., Mortelmans, L., Verbruggen, A., and Bormans, G. (2008) Synthesis and evaluation of 18F- and 11C-labeled phenyl-galactopyranosides as potential probes for *in vivo* visualization of LacZ gene expression using positron emission tomography. *Bioconjugate Chem. 19*, 441-449.
(29) Su, Y. C., Cheng, T. C., Leu, Y. L., Roffler, S. R., Wang, J. Y., Chuang, C. H., Kao, C. H., Chen, K. C., Wang, H. E., and Cheng, T. L. (2014) PET imaging of β-glucuronidase activity by an activity-based 124I-trapping probe for the personalized glucuronide prodrug targeted therapy. *Mol. Cancer Ther. 13*, 2852-2863.
(30) Antunes, I. F., Haisma, H. J., Elsinga, P. H., Sijbesma, J. W., van Waarde, A., Willemsen, A. T., Dierckx, R. A., and de Vries, E. F. (2012) *In vivo* evaluation of [18F]FEAnGA-Me: a PET tracer for imaging β-glucuronidase (β-GUS) activity in a tumor/inflammation rodent model. *Nucl. Med. Biol. 39*, 854-863.
(31) Antunes, I. F., Haisma, H. J., Elsinga, P. H., van Waarde, A., Willemsen, A. T., Dierckx, R. A., and de Vries, E. F. (2012) *In vivo* evaluation of 1-O-(4-(2-fluoroethyl-carbamoyloxymethyl)-2-nitrophenyl)-O-β-D-glucopyronuronate: a positron emission tomographic tracer for imaging β-glucuronidase activity in a tumor/inflammation rodent model. *Mol. Imaging. 11*, 77-87.
(32) Antunes, I. F., Haisma, H. J., Elsinga, P. H., Dierckx, R. A., and de Vries, E. F. (2010) Synthesis and evaluation of [18F]-FEAnGA as a PET tracer for beta-glucuronidase activity. *Bioconjugate Chem. 21*, 911-920.
(33) Kodibagkar, V. D., Yu, J., Liu, L., Hetherington, H. P., and Mason, R. P. (2006) Imaging β-galactosidase activity using 19F chemical shift imaging of LacZ gene-reporter molecule 2-fluoro-4-nitrophenol- β-D-galactopyranoside. *Magn. Reson. Imaging 24*, 959-962.
(34) Louie, A. Y., Huber, M. M., Ahrens, E. T., Rothbaucher, U., Moats, R., Jacobs, R. E., Fraser, S. E., and Meade, T. J. (2000) *In vivo* visualization of gene expression using magnetic resonance imaging. *Nat. Biotechnol. 18*, 321-325.
(35) Duimstra, J. A., Femia, F. J., and Meade, T. J. (2005) A gadolinium chelate for detection of beta-glucuronidase: a self-immolative approach. *J. Am. Chem. Soc. 127*, 12847-12855.
(36) Sherry, A. D., and Woods, M. (2008) Chemical exchange saturation transfer contrast agents for magnetic resonance imaging. *Annu. Rev. Biomed. Eng. 10*, 391-411.
(37) Yoo, B., and Pagel, M. D. (2006) A PARACEST MRI contrast agent to detect enzyme activity. *J. Am. Chem. Soc. 128*,14032-14033.
(38) Yoo, B., Raam, M. S., Rosenblum, R. M., and Pagel, M. D. (2007) Enzyme-responsive PARACEST MRI contrast agents: a new biomedical imaging approach for studies of the proteasome. *Contrast Media Mol. Imaging 2*, 189-198.
(39) Li, Y., Sheth, V. R., Liu, G., and Pagel, M. D. (2011) A self-calibrating PARACEST MRI contrast agent that detects esterase enzyme activity. *Contrast Media Mol. Imaging 6*, 219-228.
(40) Yoo, B., Sheth, V. R., and Pagel, M. D. (2009) An amine-derivatized, DOTA-loaded polymeric support for Fmoc solid phase peptide synthesis. *Tetrahedron Lett. 50*, 4459-4462.
(41) Hingorani, D. V., Randtke, E. A., and Pagel, M. D. (2013) A catalyCEST MRI contrast agent that detects the enzyme-catalyzed creation of a covalent bond. *J. Am. Chem. Soc. 135*, 6396-6398.
(42) Hingorani, D. V., Montano, L. A., Randtke, E. A., Lee, Y. S., Cárdenas-Rodríguez, J., and Pagel, M. D. (2016) A single diamagnetic catalyCEST MRI contrast agent that detects cathepsin B enzyme activity by using a ratio of two CEST signals. *Contrast Media Mol. Imaging 11*, 130-138.
(43) Fernández-Cuervo, G., Sinharay, S., and Pagel, M. D. (2016) A catalyCEST MRI contrast agent that can simultaneously detect two enzyme activities. *Chembiochem 17*, 383-387.
(44) Yoo, B., Sheth, V. R., Howison, C. M., Douglas, M. J. K., Pineda, C. T., Maine, E. A., Baker, A. F., and Pagel, M. D. (2014) Detection of *in vivo* enzyme activity with catalyCEST MRI. *Magn. Reson. Med. 71*, 1221-1230.
(45) Sinharay, S., Randtke, E. A., Jones, K. M., Howison, C. M., Chambers, S. K., Kobayashi, H., and Pagel, M. D. (2016) Noninvasive detection of enzyme activity in tumor models of human ovarian cancer using catalyCEST MRI. *Magn. Reson. Med.* Epub ahead of print. doi: 10.1002/mrm.26278
(46) Yang, X., Song, X., Li, Y., Liu, G., Ray Banerjee, S., Pomper, M. G., and McMahon, M. T. (2011) Salicylic acid and analogues as diaCEST MRI contrast agents with highly shifted exchangeable proton frequencies. *Angew. Chem. Int. Ed. 52*, 8116-8119.
(47) Harisma, H. J., Boven, E., van Muijen, M., de Jong, J., van der Vijgh, W. J. F., and Pinedo, H. M. (1992) A monoclonal antibody-beta glucuronidase conjugate as activator of the prodrug epirubicin-glucuronide for specific treatment of cancer. *Cancer 66*, 474-478.
(48) Withers, S. G. (1999) 1998 Hoffmann La Roche Award Lecture – Understanding and expoiting glycosidases *Can. J. Chem. 77* 1-11.
(49) Richard, J. P. Westerfeld, J. G., Lin, S., and Beard, J. (1995) Structure – Reactivity Relationships for β-galactosidase (*Escherichia coli*, lac Z). 2. Reactions of the Galactosyl – Enzyme Intermediate with Alcholos and Azide Ion. *Biochemistry 34,* 11713-11724.
(50) Yu, J. X., Otten, P., Ma, Z., Cui, W., Liu, L., and Mason R. P. (2004) A Novel NMR Platform for Detecting Gene Transfection: Synthesis and Evaluation of Fluorinated Phenyl β-*D*-Galactosides with Potential Application for Assessing LacZ Gene Expression. *Bioconj Chem. 15,* 1334–1341.
(51) Alouane, A., Labruére, R., Le Saux, T., Schmidt, F., and Jullien L. (2015) Self-immolative spacers: kinetic aspects, structure-property relationships, and applications. *Angew. Chem. Int. Ed. Engl. 54*, 7492-7509.
(52) Chauvin, T., Durand, P., Bernier, M., Meudal, H., Doan, B. T., Noury, F., Badet, B., Beloeil, J. C., and Tóth, E. (2008) Detection of enzymatic activity by PARACEST MRI: a general approach to target a large variety of enzymes. *Angew. Chem. Int. Ed. Engl. 47*, 4370-4372.
(53) Chauvin, T., Torres, S., Rosseto, R., Kotek, J., Badet, B., Durand P., and Tóth, E. (2012) Lanthanide (III) complexes that contain a self-immolative arm: potential enzyme responsive contract agents for magnetic resonance imaging. *Chem. Eur. J. 18*, 1408-1418.
(54) Randtke, E. A., Chen, L. Q., Corrales, L. R., and Pagel, M. D. (2014) The Hanes-Woolf linear QUESP method improves the measurements of fast chemical exchange rates with CEST MRI. *Magn. Reson. Med. 71*, 1603-1612.
(55) Randtke, E. A., Chen, L. Q., and Pagel, M. D. (2014) The reciprocal linear QUEST analysis method facilitates the measurements of chemical exchange rates with CEST MRI. *Contrast Media Mol. Imaging 9*, 252-258.
(56) Ali, M. M., Liu, G., Shah, T., Flask, C. A., and Pagel, M. D. (2009) Using two chemical exchange saturation transfer magnetic resonance imaging contrast agents for molecular imaging studies. *Acc. Chem. Res. 42*, 915-924.
(57) Karunairatnam, M. C., and Levvy, G. A. (1949) The inhibition of β-glucuronidase by saccharic acid and the role of the enzyme in glucuronide synthesis. *Biochem. J. 44*, 599-604.

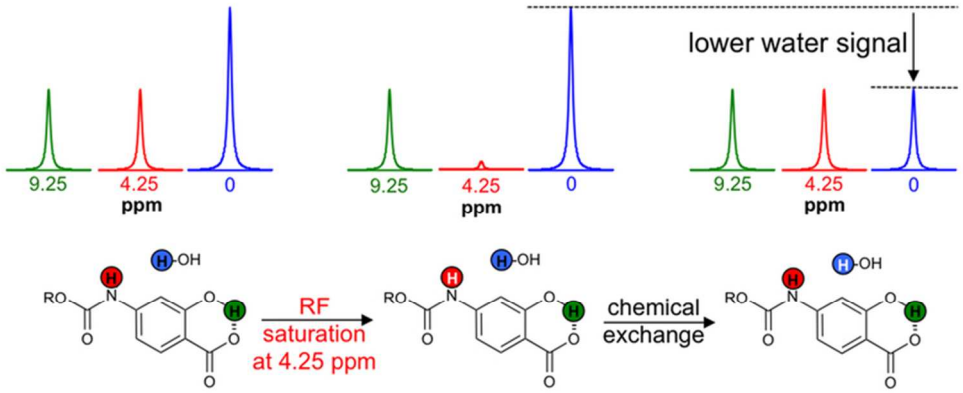

Figure 1. CEST MRI Mechanism. Radio frequency saturation of the carbamide hydrogen atom (green) results in the loss of the MRI signal (a saturated proton is shown in white). After exchanging this saturated hydrogen atom with a hydrogen atom on water (blue), some of the MRI signal of water is lost, which can be measured with MRI. The MRI signal of the proton of the salicylic acid moiety (green) is unchanged because chemical exchange with saturated carbamide or saturated water protons is negligible. However, radio frequency saturation of the salicylic acid proton would cause a similar decrease in the water signal based the same mechanism.

68x31mm (300 x 300 DPI)

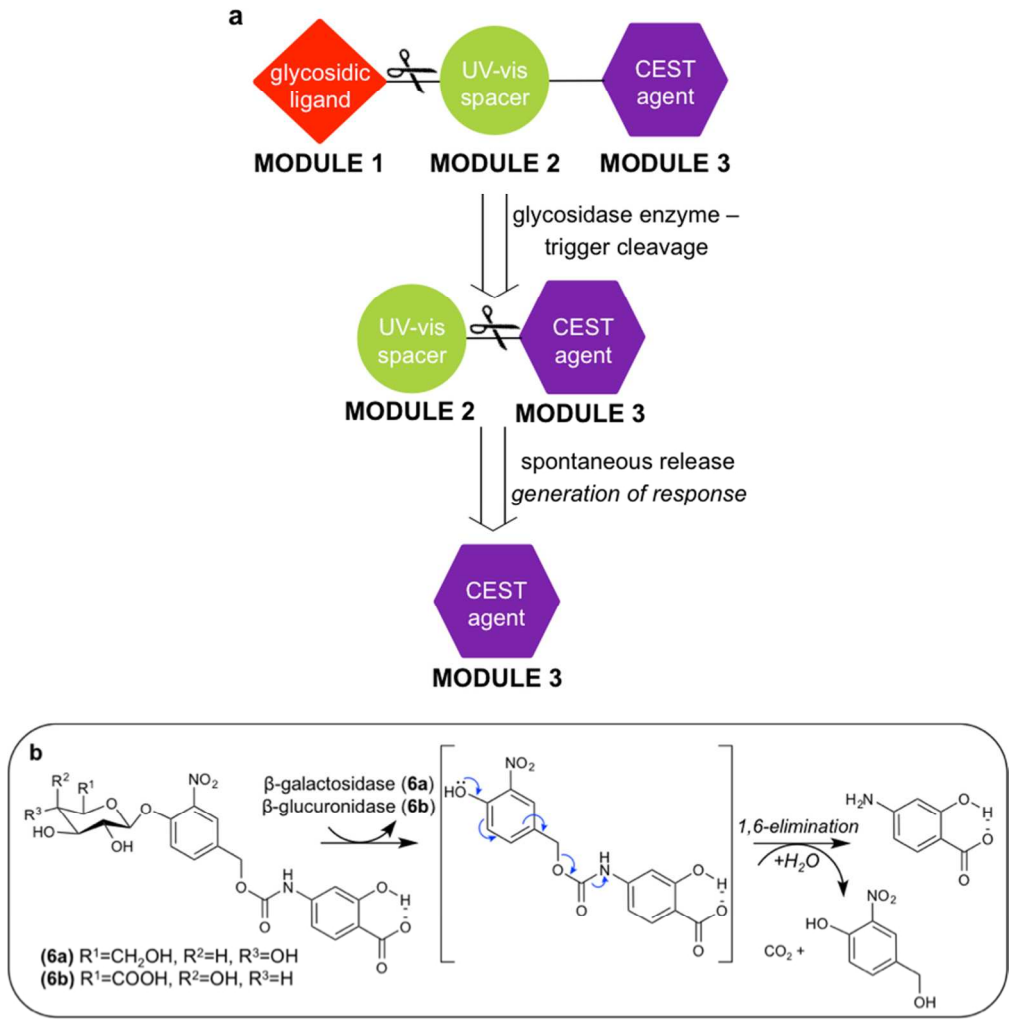

Scheme 1. (a) Modular design of the CEST MRI agent. (b) The proposed release mechanism of the enzyme responsive contrast agent.

104x107mm (300 x 300 DPI)

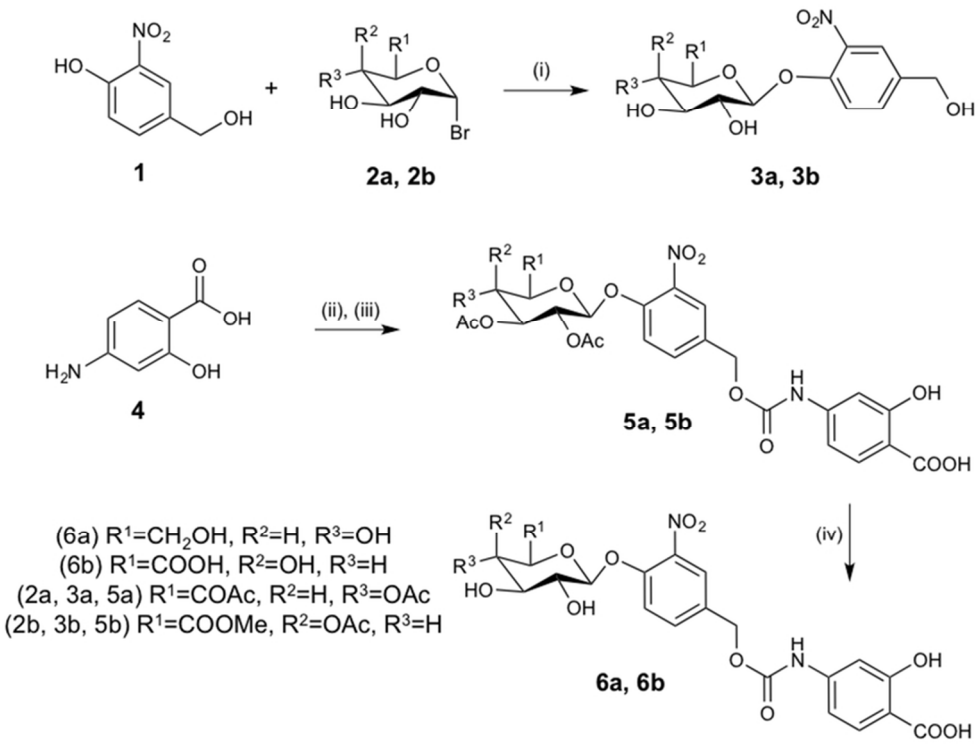

Scheme 2. (i) Silver oxide, ACN, room temperature, 2 h, 86% (3a), 88% (3b). (ii) Triphosgene, 1:1 ACN/toluene, 60 oC to 80 oC, 2h. (iii) 3, 80 oC, 1 h, 13% (5a), 34% (5b). (iv) MeOH, NaOMe, room temperature, 30 min, 47% (6a), 83% (6b).

75x55mm (300 x 300 DPI)

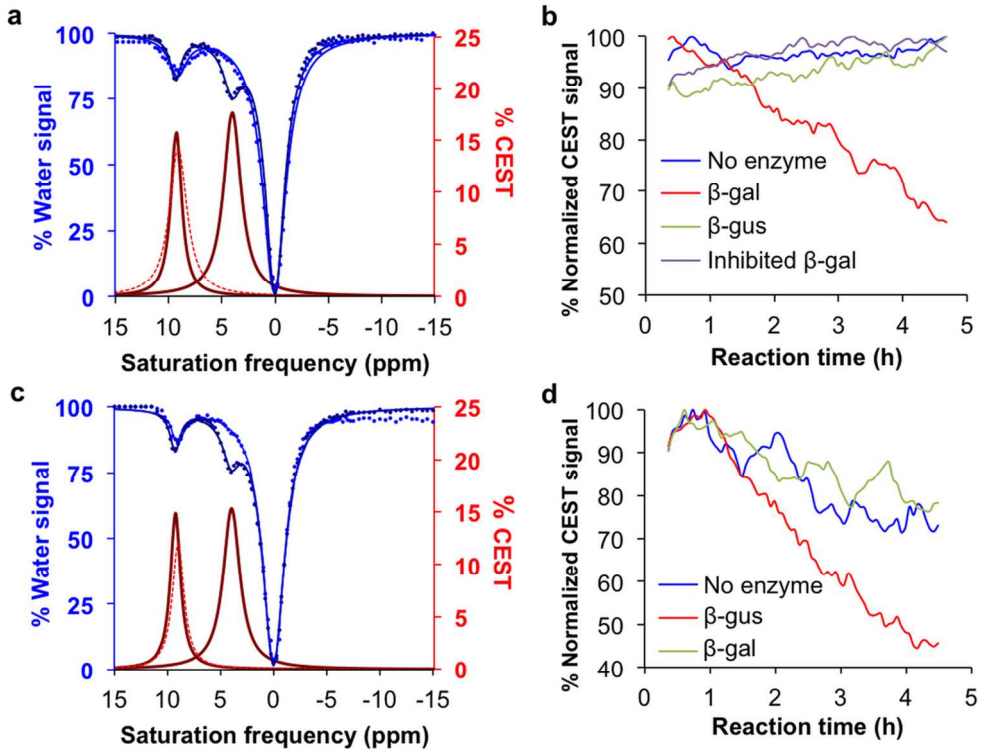

Figure 2. catalyCEST MRI. (a) The experimental CEST spectra (blue circles), the Lorentzian line fitting of the experimental CEST spectra (blue lines), and the Lorentzian line shapes showed two CEST signals from the substrate 6a (solid red lines) and only one CEST signal for the product after β-gal catalysis (dashed red line). (b) The normalized CEST signal at 4.25 ppm decreased after treatment of 6a with β-gal (red). No change in CEST signal was observed after treatment with β-gus (green), with β-gal inhibited by PETG (purple), or in the absence of enzyme (blue). (c) and (d) Similar results were obtained before and after enzyme catalysis of 6b with β-gus.

118x92mm (300 x 300 DPI)

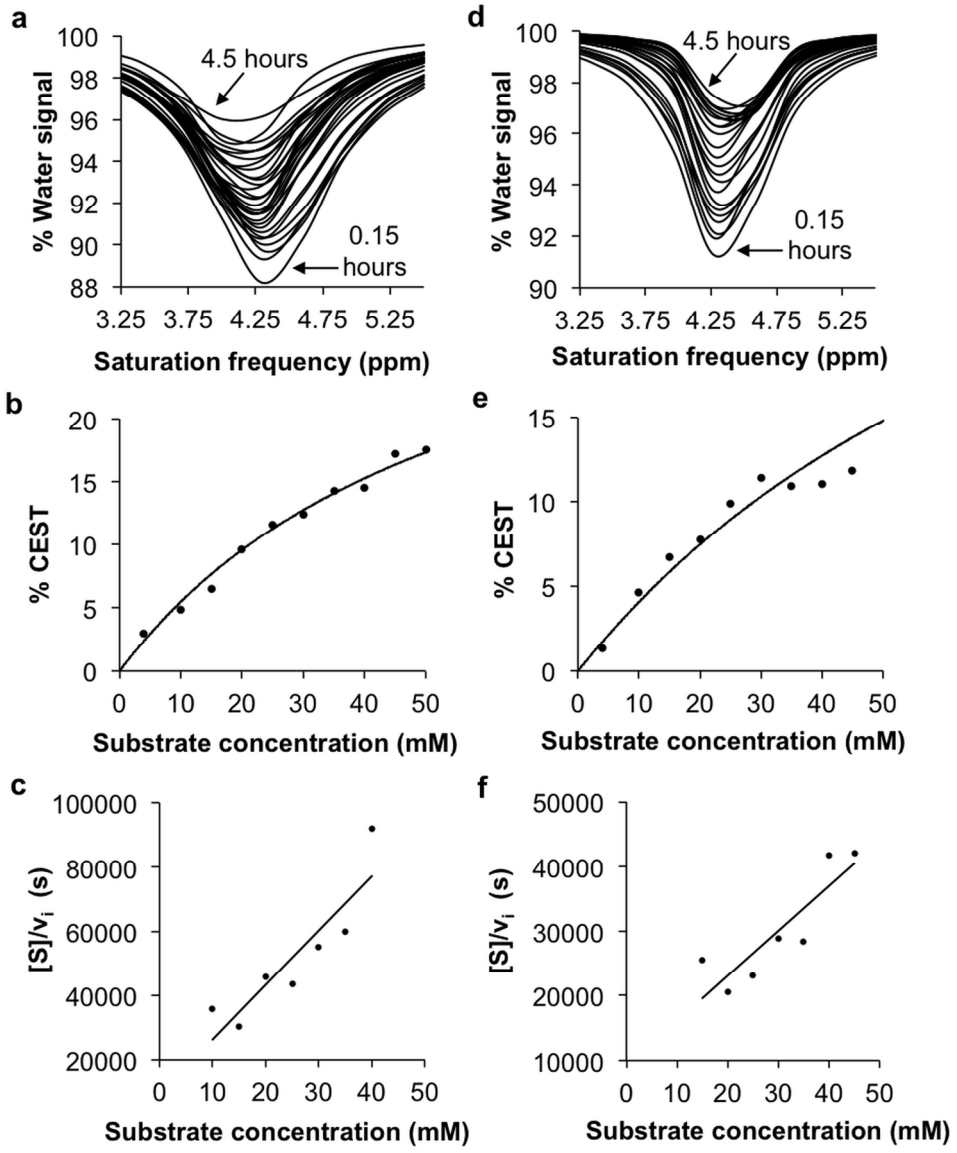

Figure. 3 Michaelis-Menten kinetics studies with catalyCEST MRI. (a) The decrease of the CEST signal at 4.25 ppm was monitored for 4.5 hours with catalyCEST MRI after adding 0.25 units of β-gal to 25 mM of 6a. (b) The CEST signal amplitude was correlated with the concentration of 6a using the HW-Conc analysis method. The initial velocity, vi, was determined by converting the CEST signal in panel a to concentration, using the calibration curve in panel b. (c) A Hanes-Woolf plot was used to determine Michaelis-Menten kinetics parameters. (d-f) This analysis was repeated for evaluating the kinetics of β-gus with its substrate 6b.

152x189mm (300 x 300 DPI)

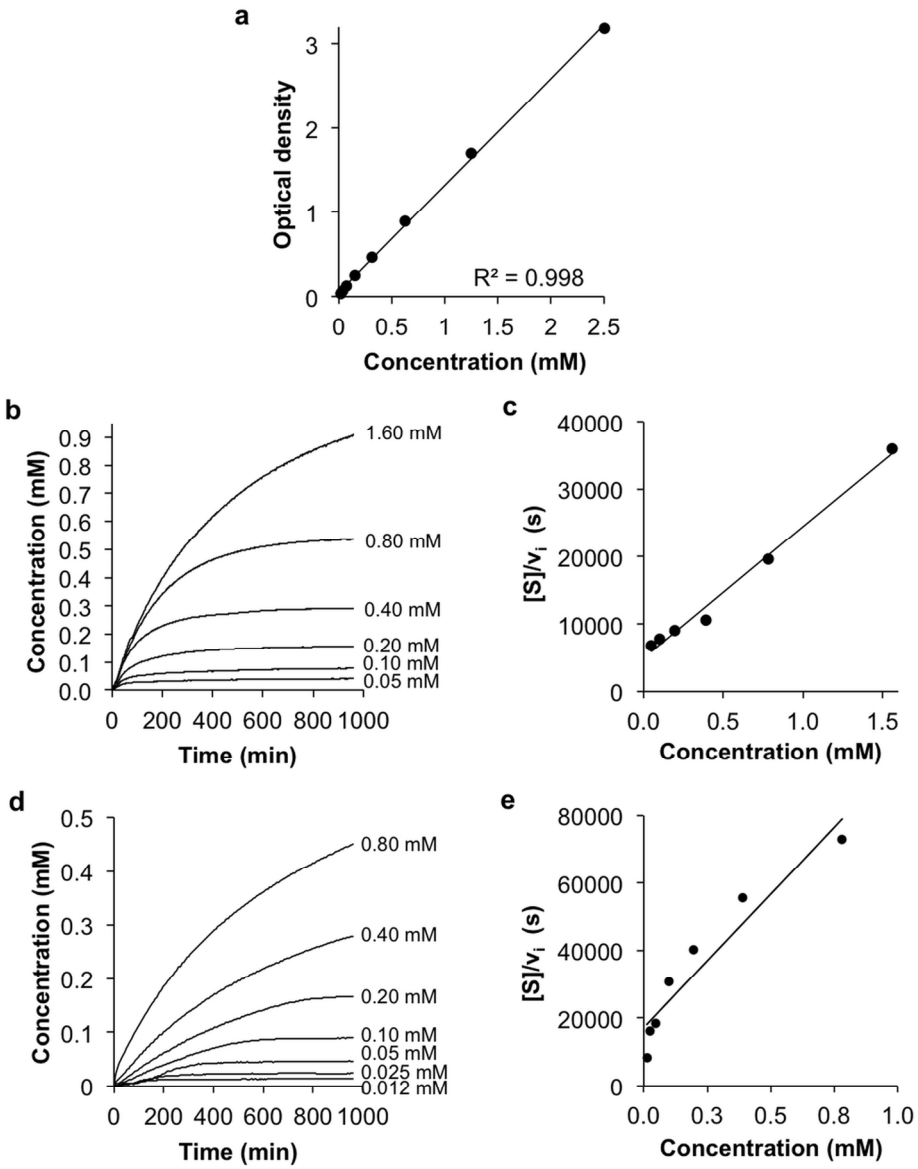

Figure. 4 Michaelis-Menten kinetics studies with absorbance at 425 nm. (a) The absorbance at 425 nm was correlated with the concentration of 4-hydroxy-3-nitrobenzyl alcohol (1) using the Beer-Lambert law. (b) The initial velocity, vi, was determined by monitoring the change in UV absorbance of 6a after adding β-gal enzyme, and converting the absorbance at 425 nm to concentration using the calibration in panel a. (c) A Hanes-Woolf plot with initial velocities and substrate concentrations was used to determine Michaelis-Menten kinetics parameters. (d) and (e) This analysis was repeated for evaluating the kinetics of β-gus with its substrate 6b.

124x153mm (300 x 300 DPI)